Paper # F20 **Topic: Soot**

5^{th} US Combustion Meeting
Organized by the Western States Section of the Combustion Institute
and Hosted by the University of California at San Diego
March 25-28, 2007.

Parameter free aggregation model for soot formation

G. Blanquart and H. Pitsch

Department of Mechanical Engineering
Stanford University, Stanford, USA

In this article we present a parameter free aggregation model for soot formation. Each soot particle is represented as a fractal aggregate that can be described by its total volume, total surface, and number of hydrogenated sites on its surface. The moments of the joint Probility Density Function (PDF) of these three quantities are solved using the Direct Quadrature Method of Moments (DQMOM). This method allows for an accurate prediction of the moments without the cost of expensive methods like Direct Simulation Monte-Carlo (DSMC). The source terms for the transport equations include nucleation, coagulation, condensation, surface growth, and oxidation. The model, referred to as Volume-Surface-Hydrogen (VSH), is applied insimulations of a series of rich laminar premixed flames. The model is able to predict soot volume fraction and primary particle diameter with good accuracy. Furthermore, it also gives insight into the surface reactivity of soot particles at high temperatures.

1 Introduction

Soot is formed in many industrial devices, such as furnaces, but also in automotive and aircraft engines, and in fires. It is commonly assumed that the inception of soot particles occurs by the collision of heavy Polycyclic Aromatic (PAH) molecules [1]. The particles further grow by collision with other particles or by addition of mass on the surface through chemical reactions [2]. Experimental observations [3, 4] suggest that soot particles are aggregates, and are composed of a certain number of small spherical particles called primary particles. These primary particles are arranged in ways that produce fractal shaped soot aggregates.

The fractal dimension of soot aggregates has been studied both experimentally and numerically in detail for different regimes. Mitchell and Frenklach [5, 6] studied the coagulation of spherical particles onto a so called collector particle. The work was performed in the free molecular regime with the incoming candidate particles having random ballistic trajectories characteristic of small particles (or large Knudsen number $\mathrm{Kn} \gg 1$). The results showed that in the limit of no surface reaction, the aggregates have a very compact structure with a rather high fractal dimension $\mathrm{D_f} \approx 2.97$, close to the results of the early work of Meakin et al. [7] ($\mathrm{D_f} \approx 3.09$). However, the high fractal dimension determined by these simulations is much higher than any of the experimental values. The reason for thos could be the assumption that every collision leads to an aggregate, especially given the fact that the colliding particles used in those simulations were very small (a few nanometers and below) and could be associated with large PAH. Those large PAH would most likely stick on the surface and render the particle more spherical.

More recently, high fidelity simulations of cluster-cluster aggregation were perfomed [8, 9]. Schmid et al. [9] considered coagulation and sintering in the so-called Diffusion Limited Cluster Aggregation regime (or DLCA), which is equivalent to the continuum regime characterized by Brownian random diffusion (small Knudsen number $\mathrm{Kn} \ll 1$). They found that in the limit of no sintering, the fractal dimension reaches a value close to $\mathrm{D_f} \approx 1.86$.

Köylü et al. [3] studied the fractal dimension of soot aggregates from turbulent non-premixed flames of acetylene, propylene, ethylene, and propane. Their measurements for the fractal properties of soot yield $D_f = 1.82$. A more recent analysis of soot fractal properties in JP-8 pool fires [4] revealed slightly lower values for the fractal dimension $1.68 < D_f < 1.72$. Most of the experimental measurements were performed on relatively large soot aggregates with diameter of their primary particles ranging from $20\,\mathrm{nm}$ to $70\,\mathrm{nm}$, and number of primary particles reaching hundreds or thousands.

Some of the soot models available in the literature have an empirical way of handling aggregation [10]. Below a certain presumed threshold diameter, soot particles are assumed to be sperical, while beyond this diameter, they are assumed to be aggregates. This approach of aggregation is limited in a sense that, as an example, the approach cannot accurately describe the population of soot particles at a time where small spherical particles are mixed with large aggregates.

Because of the vast diversity of the particle sizes and shapes found in a typical flame, a correct description of the Particle Size Distribution Function is required (PSDF). Direct Simulation Monte-Carlo (DSMC) have been shown to predict with good accuracy the full PSDF of soot [11, 12]. Results from DSMC also compared favorably with experimental measurements of the PSDF from laminar ethylene flames [13, 14]. However, the inherent cost of using DSMC for such simulations renders impossible its use for $3\mathrm{D}$ or even $1\mathrm{D}$ simulations.

Recently, Marchisio and Fox [15] applied the Direct Quadrature Method of Moments to soot formation. Rather than assuming the full form of the PSDF or simulating it completely, this method approximates the PSDF by a series of delta functions. This method proved to be effective in predicting the main moments of the PSDF, such as the volume, the surface area, or the number density. Furthermore, this method was found to be inexpensive in comparison to DSMC.

The intent of the present work is to develop a new aggregation soot model free of a priori parameters. The model is formulated in the context of DQMOM, since the ultimate goal is to apply the new soot model to a $3D$ turbulent simulation. The detailed chemical reaction mechanism used in the present study is briefly described in the foloowing section. Then, the soot model is presented, and all of the source terms are modeled. Finally, comparison with experimental measurements for a series of laminar premixed ethylene flames is provided.

2 Reaction Mechanism

The reaction mechanism used for the present study includes 140 species and 1513 reactions. The current mechanism is based on the GRI 3.0 mechanism [16]. This mechanism was originally developed for natural gas, and thus lacks the chemistry for larger molecules. As a consequence, the current mechanism has been supplemented with additional reactions relevant to C_2H_x fuels [17], and to C_3H_x and C_4H_x fuels [18].

The PAH chemistry is based on the original work of Wang and Frenklach [19–21]. Blanquart and Pitsch [22] recently recomputed and extended the database of thermodynamic properties for PAH molecules to include Cyclo-Pentafused PAH (CP-PAH) larger than acenaphthylene. The geometric structures were optimized using density functional theory with the B3LYP/6-31G++(d,p) functional. The enthalpies of formation were computed with G3(MP2)//B3, and group corrections were applied to better predict the experimental values. In addition, several of the enthalpies of formation of PAH have been updated to account for newer experimental or quantum simulation data.

3 Soot Model

3.1 Soot Representation

Experimental observations suggest that soot particles are aggregates and are composed of a certain number of small spherical particles called primary particles. These primary particles are arranged to form a fractal shaped soot aggregate. While the shape, composition and mass of these soot aggregates might not be the same from one flame to another, several assumptions have to be made so that the dimensionality of the problem is reduced.

It is first assumed that all primary particles within one aggregate have the same diameter, thereafter referred to as d_p. In a flame, it is likely that those spherical particles within one given aggregate have been formed at the same time, and hence have similar diameters. However, there is no restriction as for the change of diameter between different soot aggregates. A soot aggregate is composed of a certain number of these primary particles n_p. Given the number of primary particles per aggregate, the total volume of one soot aggregate can be expressed as

$$V = \frac{\pi}{6} n_p d_p^3 \tag{1}$$

and the total surface area as

$$S = \pi n_p d_p^2. \tag{2}$$

Given the total volume and total surface area of one soot aggregate, one can hence reconstruct the primary particle diameter and the number of primary particles per aggregate as follows:

$$d_p = 6\frac{V}{S} \tag{3}$$

$$n_p = \frac{1}{36\pi} S^3 V^{-2} \tag{4}$$

The density of soot particles is considered to be constant and independent of the size and shape of the aggregate. The value used in the present work is $\rho_s = 1800\,\mathrm{kg/m^3}$. Finally, it is assumed that only carbon atoms contribute to the mass of soot particles. In reality, soot particles are composed of several different elements, with carbon and hydrogen being the two predominant atoms. Experimental measurements have reported that the $\mathrm{C/H}$ molar ratio can be much greater than unity[4, 23]. Given the molecular weight of carbon and hydrogen, neglecting hydrogen atoms when evaluating the mass of soot particles is a reasonable assumption.

As a consequence, in the present model, a soot particle would be described by two parameters: the total volume (V) and total surface area (S). However, to better predict the soot volume fraction over a wide range of temperatures and pressures, a third parameter is introduced. This third quantity is the number of hydrogenated carbon sites on the surface of the soot aggregate, denoted H. We will refer to this model subsequently as Volume-Surface-Hydrogen (VSH) model.

3.2 Direct Quadrature Method of Moments

To accurately describe the number density function of soot, the Direct Quadrature Method of Moments (DQMOM) is used [15]. Let us consider the Population Balance Equation (PBE):

$$\frac{\partial n}{\partial t} + \frac{\partial}{\partial x_j}\left(u_j n\right) - \frac{\partial}{\partial x_j}\left(D\frac{\partial n}{\partial x_j}\right) = \dot{S}\,, \tag{5}$$

where $n = n(V, S, H; \mathbf{x}, t)$ is the number density of soot particles having a given volume V, a given surface S, and a given number of hydrogenated sites H. This number density varies in time and space. The source term $\dot{S}$ that appears in the PBE is a function of this number density function. One is generally not interested in the full form of the number density function, but only in some of its moments defined as

$$M_{k_1,k_2,k_3}(\mathbf{x}, t) = \int_V \int_S \int_H V^{k_1} S^{k_2} H^{k_3} n(V, S, H; \mathbf{x}, t) dH dS dV. \tag{6}$$

For instance, predicting accurately the total volume ($M_{1,0,0}$), the total surface area ($M_{0,1,0}$), and the total number density ($M_{0,0,0}$) is generally quite important. From Eq. 5, evolution equations for the moments can be written, in which the source terms are given by

$$\dot{S}_{k_1,k_2,k_3}(\mathbf{x}, t) = \int_V \int_S \int_H V^{k_1} S^{k_2} H^{k_3} \dot{S}(V, S, H; \mathbf{x}, t) dH dS dV \tag{7}$$

The closure of these source terms is performed by quadrature approximation of higher order. The number density of soot particles is approximated by a set of delta functions:

$$n(V, S, H; \mathbf{x}, t) \approx \sum_{\alpha=1}^{n_d} w_\alpha(\mathbf{x}, t)\delta_\alpha\left(V - V_\alpha(\mathbf{x}, t)\right)\delta_\alpha\left(S - S_\alpha(\mathbf{x}, t)\right)\delta_\alpha\left(H - H_\alpha(\mathbf{x}, t)\right) \tag{8}$$

with n_d the number of delta functions used for the quadrature. The weights, $w_\alpha(\mathbf{x}, t)$ and the abscissas, $V_\alpha(\mathbf{x}, t)$, $S_\alpha(\mathbf{x}, t)$, and $H_\alpha(\mathbf{x}, t)$ of the delta functions also vary with time and space. Using this expression, the source terms for the moments are approximated by

$$\dot{S}_{k_1,k_2,k_3} \approx \sum_{\alpha=1}^{n_d} V_\alpha^{k_1} S_\alpha^{k_2} H_\alpha^{k_3} \dot{S}(V_\alpha, S_\alpha, H_\alpha) w_\alpha \tag{9}$$

This method is called the Quadrature Method of Moments (QMOM). With the quadrature approximation, the evolution equations for the moments are closed entirely. However, one has to know how to recompute the n_d weights and $3n_d$ abscissas given a set of $4n_d$ moments. The product-difference algorithm can be used in the case of a monovariate number density function [24]. However, in the case of a multivariate number density function, no such algorithm exists.

The DQMOM method solves for the weights and abscissas directly rather than for the moments. By replacing the number density appearing in the PBE (Eq. 5) with the aproximated form given by Eq. 8, transport equations for the weights and abscissas are obtained:

$$\frac{\partial w_\alpha}{\partial t} + \frac{\partial}{\partial x_j}\left(u_j w_\alpha\right) - \frac{\partial}{\partial x_j}\left(D\frac{\partial w_\alpha}{\partial x_j}\right) = \dot{a}_\alpha \,, \tag{10}$$

$$\frac{\partial w_\alpha \xi_\alpha}{\partial t} + \frac{\partial}{\partial x_j}\left(u_j w_\alpha \xi_\alpha\right) - \frac{\partial}{\partial x_j}\left(D\frac{\partial w_\alpha \xi_\alpha}{\partial x_j}\right) = \dot{b}_\alpha \,, \tag{11}$$

where ξ_α can be any one of the three abscissas (V_α, S_α, or H_α). One can show that the source terms ($\dot{a}_\alpha$ and $\dot{b}_\alpha$) are solutions of a linear system, whose right-hand side is exactly the source terms for the set of $4n_d$ moments [15]. The matrix involved in the linear system only depends upon the abscissas of the n_d delta functions.

As a consequence, the source terms are first computed for a given set of moments of the number density function ($\dot{S}_{k_1,k_2,k_3}$). Then, a linear system is solved to obtain the source terms for the weights and abscissas ($\dot{a}_\alpha$ and $\dot{b}_\alpha$). The transport equation for the weghts and abscissas (Eq. 10 and 11) are solved using those source terms. Finally, the moments of the PSDF are reconstructed using Eq. 6.

3.3 Source terms

3.3.1 Nucleation

Nucleation of soot particles is modeled as the collision and subsequent coalescence of two heavy PAH molecules. Since simulating every possible PAH species encountered in typical flames is not possible, it is assumed that the rate of nucleation is given by the rate of formation of some smaller PAH molecules. Those species include the largest species which is solved for as part of the gas phase (first nucleation path - Fig. 1), and other species formed according to Violi's mechanism [25–27] (second nucleation path - Fig. 2). While the first nucleation path produces PAH molecules of a given structure and size (cyclo[cd]pyrene $C_{18}H_{10}$), the second path produces molecules of different shapes and sizes. Figure 2 shows two typical molecules formed in this second nucleation path. Those molecules originate from the addition reaction of a radical aromatic species (like A_1*, A_2*,..., referred as $\mathrm{Arom}*$) on a cyclopentafused aromatic molecule (like $\mathrm{A}_2\mathrm{R5}$, referred as $\mathrm{CP-Arom}$). The reactions of formation of PAH species for the two paths are assumed to be irreversible and their rates are given in table 1.

Rather than computing all possible PAH molecular structures, here only the total rate of formation of PAH molecules, the average carbon, and the average hydrogen contents per molecule are evaluated. From these quantities, average volume (V), surface area (S) and number of hydrogen sites (H) are expressed for the soot particle resulting from the collision of two PAH molecules. In this procedure, it is assumed that the newly formed soot particle is purely spherical ($n_p = 1$), has the density of soot and that all hydrogen atoms are located on the surface. In other words, all hydrogen atoms are available for surface reactions.

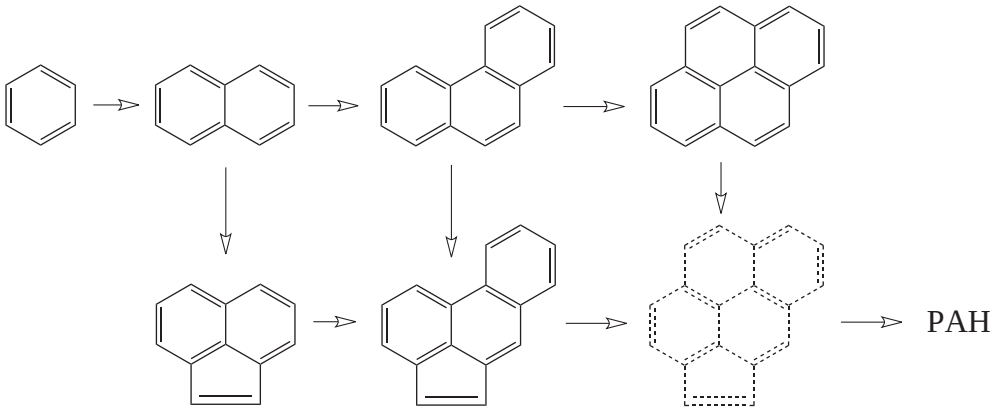

Figure 1: Aromatic growth and PAH formation following the HACA mechanism (First nucleation path).

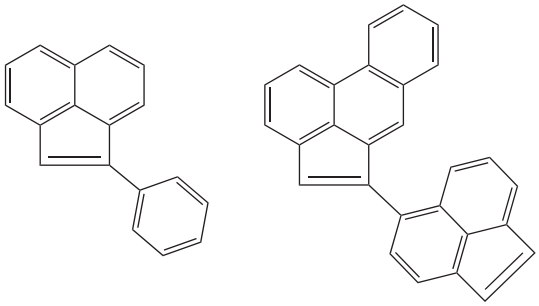

Figure 2: Typical PAH molecules formed following Violi's mechanism (Second nucleation path).

Reactions						A	n	E	Ref.
			First nucleation path						
1:	A_3R5*	+ C_2H_2	$\rightarrow$	PAH	+ H	$1.87E7$	1.79	13.65	[28]
2:	A_4*	+ C_2H_2	$\rightarrow$	PAH	+ H	$1.87E7$	1.79	13.65	[28]
3:	A_3R5	+ C_2H	$\rightarrow$	PAH	+ H	$8.33E13$	0	0	[29]
4:	A_4	+ C_2H	$\rightarrow$	PAH	+ H	$1.67E14$	0	0	[29]
			Second nucleation path						
5:	$Arom*$	+ $CP-Arom$	$\rightarrow$	PAH	+ H	$1.29E1$	3.62	0.77	[26, 27]

Table 1: Rate coefficients for the reactions of formation of PAH given in Arhenius form ($k = AT^n exp(-E/RT)$). Units are cm^3, K, mol, s and kJ.

The full source terms for the moments of the Joint PDF are then given by:

$$\dot{S}^{nucl}_{k_1,k_2,k_3} = \frac{1}{2}\beta_N \left[PAH\right]^2 V^{k_1} S^{k_2} H^{k_3} \,, \tag{12}$$

where β_N is the collision rate between two PAH molecules, and $[PAH]$ represents the concentration of PAH molecules.

3.3.2 Coagulation

The coagulation process represents the collision and subsequent coalescence of two soot particles. The rate of those collisions is a function of the size and shape of the colliding particles. Small primary particles, characterized by a large Knudsen number ($\mathrm{Kn} \gg 1$) , evolve in the free molecular regime, while large aggregates, characterized by a small Knudsen number, evolve in the continuum regime ($\mathrm{Kn} < 1$). Kazakov & Frenklach [30] developed expressions for the collision rates for the free molecular ($\beta^{f.m.}_{i,j}$) and for the continuum regimes ($\beta^{cont.}_{i,j}$)

$$\beta^{f.m.}_{i,j} = 2.2\sqrt{\frac{\pi kT}{2m_{ij}}}\left(d_{c_i} + d_{c_j}\right)^2 \,, \tag{13}$$

$$\beta^{cont.}_{i,j} = \frac{2kT}{3\mu}\left(\frac{C_i}{d_{m_i}} + \frac{C_j}{d_{m_j}}\right)\left(d_{c_i} + d_{c_j}\right) \,, \tag{14}$$

where $m_{ij} = \frac{m_i m_j}{m_i + m_j}$ is the reduced mass, μ the dynamic viscosity of the surrounding gas, d_{c_i}, d_{c_j} are the collision diameters, and d_{m_i}, d_{m_j} the mobility diameters. The Cunningham slip correction factor takes the form $C_i = 1 + 1.257\mathrm{Kn}_i$ with the Knudsen number expressed as $\mathrm{Kn}_i = \lambda / d_{c_i}$. The collision rate in the transition regime is approximated by the harmonic mean of the asymptotic values [31]

$$\beta_{i,j} = \frac{\beta^{f.m.}_{i,j}\,\beta^{cont.}_{i,j}}{\beta^{f.m.}_{i,j} + \beta^{cont.}_{i,j}} \,. \tag{15}$$

Following the work of Kruis et al. [32], the collision and mobility diameters are assumed to be proportional to the radius of gyration, which is defined as:

$$R_g = k_f d_p n_p^{1/D_f} \tag{16}$$

Here, we will assume that in the limit of a single sphere, both of the collision and the mobility diameters are equal to the real diameter:

$$d_c \equiv d_m \equiv d_p n_p^{1/D_f} , \tag{17}$$

where D_f is the fractal dimension of the soot aggregates. In the present work, the fractal dimension is taken to be $D_f = 1.8$. This value corresponds to typical soot aggregates formed in premixed and diffusion flames [3, 4].

The full source terms for the moments of the Joint PDF are then given by:

$$\dot{S}^{coag}_{k_1,k_2,k_3} = \sum_{i,j=1}^{n_d} \beta_{i,j}\left(V^{k_1}_{i+_j} S^{k_2}_{i+j} H^{k_3}_{i+j} - V^{k_1}_i S^{k_2}_i H^{k_3}_i - V^{k_1}_j S^{k_2}_j H^{k_3}_j\right) w_i w_j \,, \tag{18}$$

Reactions				A	n	E	ref.
1:	$Soot-H + H$	$\leftrightarrow$	$Soot^* + H_2$	$1.00E8$	1.80	68.42	[33]
				$8.68E4$	2.36	25.46	
2:	$Soot-H + OH$	$\leftrightarrow$	$Soot^* + H_2O$	$6.72E1$	3.33	6.09	[34]
				$6.44E-1$	3.79	27.96	
3:	$Soot-H$	$\leftrightarrow$	$Soot^* + H$	$1.05E60$	-12.40	619.55	[35]
				$3.895E57$	-12.19	143.50	
4:	$Soot^* + C_2H_2$	$\rightarrow$	$Soot-H$	$3.14E7$	1.77	13.54	[28]

Table 2: Rate coefficients for the surface reactions in Arrhenius form ($\mathbf{k = AT^n exp(-E/RT)}$). Units are cm^3, K, mol, s and kJ.

where V_{i+j}, S_{i+j}, and H_{i+j} represent the total volume, total surface area and total number of hydrogenated sites of the soot particle resulting from the collision. Those quantities will be discussed in more detail later.

3.3.3 Growth by Surface Reactions

Several reactions will take place on the surface of a soot particle. In the present model, we restrict ourselves to the H-abstraction $\mathrm{C_2H_2}$-addition (HACA) mechanism[2]. In this mechanism, the addition of mass on the surface of a soot particle proceeds in several steps. Each of these steps is assigned a rate constant in the Arrhenius form as shown in table 2.

For the H-abstraction reactions, the rate constants were taken from similar reactions on benzene molecules, which were divided by a factor of 6 to account for the number of active sites[33–35]. When available, the high pressure limit of the rate constant was considered.

Accoirding to reaction 4 in table 2, the newly formed radical site on the soot surface can react with an acettlene molecule from the gas phase, and form a vinyl-substituted site. The reaction of acetylene addition has been studied recently with high fidelity quantum simulations by Richter et al.[28]. The rate constants for the acetylene addition on phenyl or naphthyl radicals are quite similar, and differ only by a constant factor. This factor comes from the interaction of the acetylene molecule with the second ring of the radical. The surface of a soot particle is a lot more complex than that of phenyl or naphthyl. As a consequence, the factor in front of the rate constant has been slightly adjusted as to better match the experimental measurements. The final rate constant is shown in table 2. In the present model, it is assumed that the reaction of acetylene addition is irreversible.

Then, several different stabilization reactions can occur. These reactions can lead to cyclopenta-fused aromatics (path 1), ethynyl substituted aromatics (path 2), or ring closure (path 3 and 4), as depicted in Fig. 3. In the present model, we do not directly distinguish these reaction pathways, since we cannot keep track of all the possible outcomes. Instead, we just consider the resulting increase or decrease of the number of hydrogenated sites on the soot surface.

The reaction of direct cyclization to form a cyclopentafused aromatic (path 1) occurs on a “zigzag” site and conserves the number of hydrogenated sites. While the two resulting sites are not aromatic sites, it has been shown that those sites can transform back into aromatic sites [36]. A stabilization

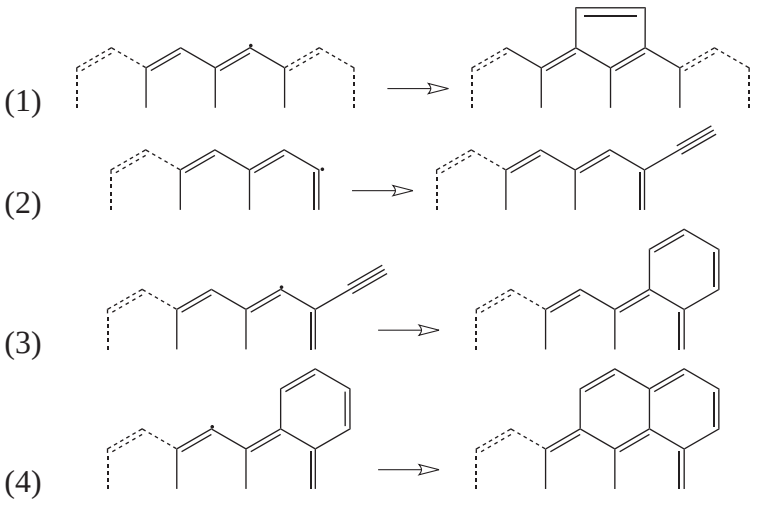

Figure 3: Possible stabilization processes resulting from the addition of acetylene C_2H_2 on a radical site.

to an ethynyl substituted aromatic (path 2) is generally followed by a second acetylene addition to form a new aromatic ring (path 3). During this process, two active hydrogenated sites are formed. However, this reaction does not occur often, since it takes place only at the corners of graphite layers. Finally ring closure can occur at a so called armchair site (path 4), which conserves the number of hydrogenated sites. This reaction path is usually assumed to be the more common path for growth by surface reaction [37]. As a consequence, it is a good approximation to consider that the total number of hydrogenated sites in a soot particle is not affected by surface reactions.

To reduce the cost of the simulation, the radical sites on the soot surface are assumed to be in quais steady-state. Then, the final rate constant is given by:

$$\dot{\omega} = k_4 \left[C_2H_2\right] \left[Soot{-}C^*\right] \tag{19}$$

with

$$\left[Soot{-}C^*\right] = \frac{r}{1+r} M_{0,0,1} \quad , \quad r = \frac{k_{1f}\left[H\right] + k_{2f}\left[OH\right] + k_{3f}}{k_{1b}\left[H_2\right] + k_{2b}\left[H_2O\right] + k_{3b}\left[H\right]} \tag{20}$$

where $M_{0,0,1}$ corresponds to the total concentration of hydrogenated cabon sites per unit volume.

Through the acetylene addition reaction, two carbon atoms are added to the mass of the particle, thus leading to an increase in the total volume of the aggregate:

$$\delta V = \frac{2W_c}{\rho_s N_A}, \tag{21}$$

where W_c is the molecular weight of carbon, N_A the Avogadro number, and ρ_s the density of soot. During this process, the total surface area of the particle is changed. Adding mass on the surface of an aggregate will slowly transform this aggregate into a more spherical particle. The number of primary particles per aggregate will decrease ($\delta\left(n_p\right) < 0$), while their diameter will increase ($\delta\left(d_p\right) > 0$). The rate of change of those two quantitites are linked. During this growth, it can be shown that the change in the collision diameter is the same as the change in the diameter of the primary particles:

$$\delta\left(d_p\right) = \delta\left(d_c\right) \tag{22}$$

Then, from Eq. 17 follows:

$$\delta\left(d_p\right) = d_c \times \left(\frac{\delta\left(n_p\right)}{n_p} + \frac{1}{D_f}\frac{d\left(d_p\right)}{d_p}\right). \tag{23}$$

As a result, the change in the total surface area can be expressed as:

$$\frac{\delta S}{S} = \frac{\delta V}{V}\left[\frac{1 - n^{1/D_f} - \frac{2}{D_f}}{1 - n^{1/D_f} - \frac{3}{D_f}}\right] \tag{24}$$

The full source term for the moments of the Joint PDF is then given by:

$$\dot{S}^{surf}_{k_1,k_2,k_3} = \frac{\dot{\omega}}{M_{0,0,1}}\sum_{i=1}^{n_d}\left(\frac{\delta V_i}{V_i} + \frac{\delta S_i}{S_i}\right) V_i^{k_1} S_i^{k_2} H_i^{k_3+1} w_i. \tag{25}$$

where δV_i and δS_i are given by Eq. 21 and Eq. 24 respectively. The change in the total number of hydrogenated sites δH_i does not appear in the source term as it is zero.

3.3.4 Condensation

Condensation corresponds to the collision of a PAH molecule with a soot aggregate. The sticking coefficient is assumed to be unity. The pool of PAH species condensing on the surface of a soot particle is the same as that previously used for nucleation. In fact nucleation and condensation are two competiting processes. It is assumed that the PAH species, which are formed from chemical reactions in the gas phase, and consummed by particle nucleation or condensation on the surface of existing soot particles, are in quasi-steady states. Since the rate of condensation is linear in the concentration of PAH species, and the rate of nucleation quadratic, we obtain a very simple equation that can be solved for the concentration of PAH species, denoted by $[PAH]$

$$\dot{\omega}_{PAH} = \beta_N \left[PAH\right]^2 + \sum_{i=1}^{n_d} \beta_{C_i} \left[PAH\right] w_i \ , \tag{26}$$

where β_{C_i} is the rate of collision of a PAH molecule with a given soot aggregate. This collision rate has the same form as that of the collision between two soot aggregates (Eq. 13, 14, and 15).

The change of total volume has a form very similar to that for surface reactions (Eq. 21), and can be written easily as a function of the number of carbon atoms in the PAH species (n_C^{PAH})

$$\delta V = \frac{n_C^{PAH} W_c}{\rho_s N_A} \, . \tag{27}$$

Since the PAH species are small in comparison to a soot aggregate, it is assumed that the change in the total surface area follows the same trend as for the growth by surface reactions (Eq. 24). However, the total number of hydrogenated carbon sites is not constant anymore, and its change is exactly equal to the number of hydrogen atoms in the colliding PAH molecule:

$$\delta H = n_H^{PAH} \tag{28}$$

The full source term for the moments of the Joint PDF is then given by:

$$\dot{S}^{cond}_{k_1,k_2,k_3} = \left[PAH\right]\sum_{i=1}^{n_d}\beta_{C_i}\left(\frac{\delta V_i}{V_i} + \frac{\delta S_i}{S_i} + \frac{\delta H_i}{H_i}\right) V_i^{k_1} S_i^{k_2} H_i^{k_3} w_i. \tag{29}$$

Reactions				A	n	E
5:	$S_A + O2$	$\rightarrow$	$S_A + 2CO$	$3.78E10$	1.00	151.00
6:	$S_B + O2$	$\rightarrow$	$S_A + 2CO$	$3.56E10$	1.00	98.00
7:	S_A	$\rightarrow$	S_B	$5.59E5$	0.50	135.56
8:	S_B	$\rightarrow$	S_A	$4.71E8$	0.50	489.00

Table 3: Rate coefficients for the oxidation reactions in Arhenius form ($k = AT^n exp(-E/RT)$). Units are cm^3, K, mol, s and kJ.

3.3.5 Oxidation

In addition to the reacstions previously mentioned in the context of surface growth mechanism, other heterogeneous reactions can occur on the particle surface. Reactions like the oxidation by O_2 or OH are very important, since they account for most of the mass loss of soot in flames. Nagle & Strickland-Constable [38] originally expressed the rate of oxidation by O_2 reactions for soot particles. Recently, Nienow et al. [39] refined the oxidation rate by proposing a new chemical mechanism (Table 3). In their refined model, as in the original NSC model, they distinguish between two possible sites on the soot surface: S_A and S_B, which they assumed to be in quasi-steady states. This mechanism is able to better represent the pressure dependence of the oxidation rate by molecular oxygen. The rate expressions used in the present work are given in table 3.

The reaction rates for the oxidation processes ($\dot{\omega}_{ox}$) are expressed as the rate for the abstraction of one carbon atom from the soot surface. When these reactions occur, the volume of a soot particle decreases according to

$$\delta V = -\frac{W_c}{\rho_s N_A}. \tag{30}$$

As in the case of surface growth by acetylene addition, the total surface area is changed. In the case of oxidation, it is assumed that the number of primary particles per aggregate remains constant throughout the oxidation process

$$d\left(n_p\right) = 0 \tag{31}$$

Following this assumption, the rate of change of the total surface can be expressed with the rate of change of the total volume. It is further assumed that the number of hydrogenated sites per unit soot surface is kept constant. As a consequence, the rate of change of the number of hydrogenated sites takes the form

$$\frac{\delta H}{H} = \frac{\delta S}{S} = \frac{2}{3}\frac{\delta V}{V}. \tag{32}$$

The full source term for the moments of the Joint PDF is then given by:

$$\dot{S}^{ox}_{k_1,k_2,k_3} = \frac{7}{3}\delta V \dot{\omega}_{ox} \frac{M_{k_1,k_2+1,k_3-1}}{M_{0,1,0}} \tag{33}$$

3.4 Surface area change by addition of mass

For all possible collisions, the total volume of the resulting particle is the sum of the volumes of the two colliding particles:

$$V_{i+j} = V_i + V_j. \tag{34}$$

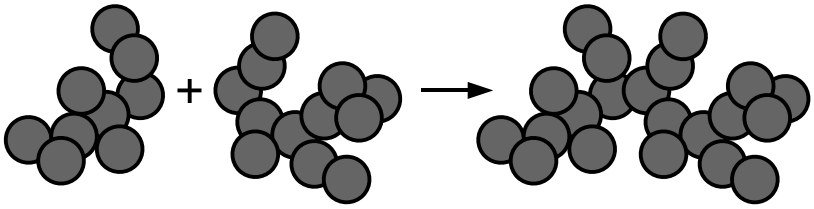

(a) Collision of two large aggregate

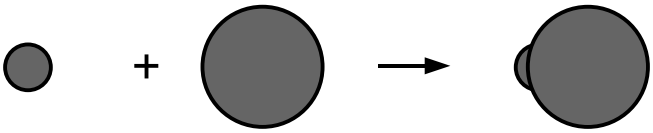

(b) Coalescence of a small particle with a large aggregate

Figure 4: Results of two extreme collision cases

However, the shape of the resulting soot particle could be very different and hence its total surface area varies a lot. Figure 4 shows two extreme collision cases. The collision between two large aggregates will lead to the formation of an even larger aggregate (Fig. 4(a)), whose total surface area is exactly the sum of the surface areas of the two colliding particles

$$S^a_{i+j} = S_i + S_j. \tag{35}$$

On the other hand, a small spherical particle (j) colliding with a large aggregate (i) will simply be absorbed into the larger particle (Fig. 4(b)). In the limit of infinitely small addition of mass ($V_j \ll V_i$), the increase of the total surface area of the large aggregate is small, and hence can be expressed as

$$S^b_{i+j} = S_i + \delta S. \tag{36}$$

where δS is given by Eq. 24 with $\delta V = V_j$ and $V = V_i$. For intermediate cases, the new total surface area is evaluated as the geometric weighted average of the two above extreme cases:

$$S_{i+j} = \left(S^a_{i+j}\right)^{\alpha} \times \left(S^b_{i+j}\right)^{(1-\alpha)} \tag{37}$$

where the weight $\alpha = V_j/V_i$ is expressed as the ratio of the smaller of the two volumes by the larger. Finally, the number of hydrogenated sites of the resulting soot particle is computed by assuming that the density of sites by unit of soot surface is constant.

4 Results

4.1 Flame Configurations

The present soot model is applied to a series of atmospheric rich premixed ethylene flames [40]. The flame parameters are given in table 4. The gas phase chemistry is solved using the FlameMaster code [41]. To better predict soot properties, and because of unknown heat losses to the wall due to conduction, the experimental temperature profiles were imposed in the computations.

The DQMOM is implemented as part of the FlameMaster code and is fully coupled with the gas phase chemistry. During simulations, the total mass of carbon atoms is conserved, since the mass

Fuel	ϕ	T_{10}
C_2H_4	1.98	$1770K$
C_2H_4	1.88	$1850K$
C_2H_4	1.78	$1880K$

Table 4: Flame parameters

transfered to the soot particles due to nucleation, condensation or surface growth is removed from the gas phase. The simulations have been performed with a quadrature approximation of order two by representing the joint particle size distribution function by two delta functions ($n_d = 2$).

Figure 5 gives a comparison of the predicted mole fractions of the main species of the gas phase with the experimental measurements. As expected, the chemical mechanism is able to predict the main combustion products (CO and CO_2), as well as intermediate species relevant for soot formation (CH_4 and C_2H_2). The latter one of these is of high importance for soot surface growth.

4.2 Volume Fraction

Figure 6 provides a comparison between predicted and measured soot volume fraction as a function of distance above the burner surface. The present soot model is able to predict quite accurately the soot volume fraction for the three flames considerd here. The deviation with the experimental profiles is less than a factor of two, which can be considered to be within the experimetal margins of error.

It is observed that the soot volume fraction decreases with increasing temperature. This is an experimentally well known and characterized phenomenon [42]. Below a certain temperature, the soot volume fraction increases with increasing temperature. Then beyong this limit temperature, the soot volume fraction decreases if the temperature is further increased. This "bell-shaped" curved has been measured experimentally for several premized flames by Böhm et al. [42]. The value of the temperature corresponding to the maximum soot yield is a function of the fuel and flame parameters.

The flames measured by Xu et al. [40] are all located in the soot fall-off region corresponding to higher temperatures. The current model is able to predict this decrease in the soot volume fraction when the temperature is increased.

Several models have been developed to account for this decrease at higher temperature [10]. Most of those models assume a given density of sites per unit soot surface $\chi \approx 2.3 \times 10^{19} m^{-2}$, and introduce a parameter α, which describes the fraction of active sites. In a recent paper, Appel et al. [10] expressed the parameter α as a function of the local temperature and the first size moment of the soot particle distribution $\mu_1 = M_{1,0,0}/M_{0,0,0}$. This fit was empirically determined from a least square approach.

The present model does not assume a given density of active sites per unit soot surface. From two of the three quantities characterizing the soot particles, the surface area (S) and the number of

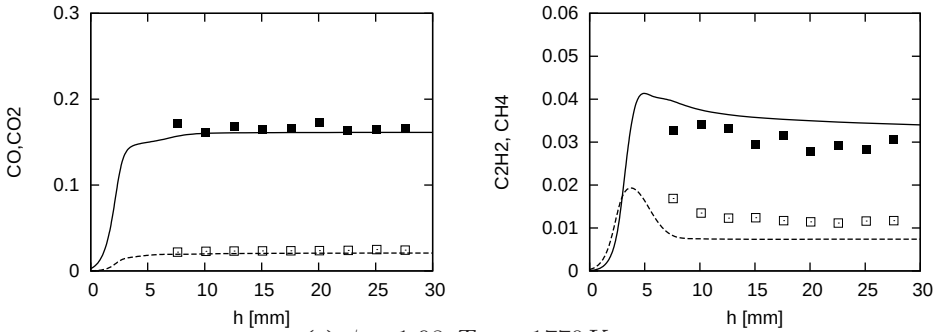

(a) $\phi = 1.98, T_{10} = 1770K$

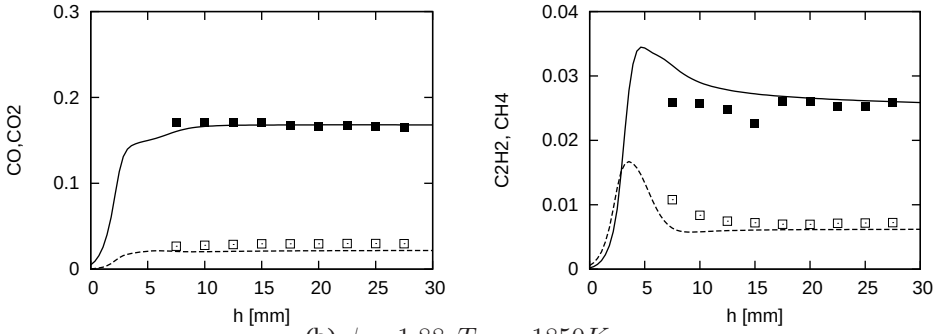

(b) $\phi = 1.88, T_{10} = 1850K$

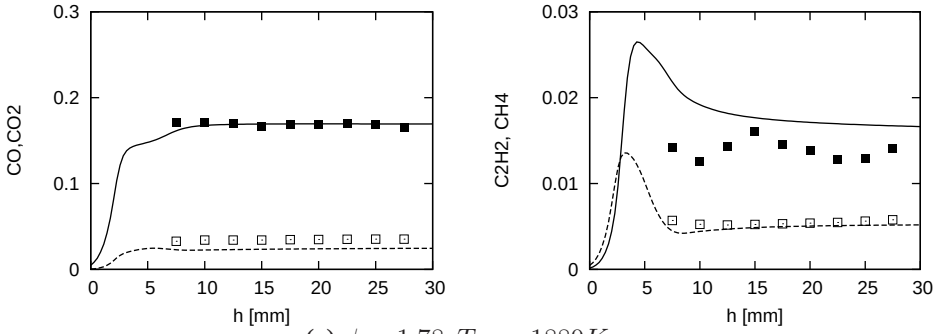

(c) $\phi = 1.78, T_{10} = 1880K$

Figure 5: Mole fractions of the main species of the gas phase predicted with the current mechanism. Symbols are experiments [40], open symbols for CO_2 and CH_4, filled symbols for CO and C_2H_2. Solid lines are either CO or C_2H_2, and dashed lines are either CO_2 or CH_4.

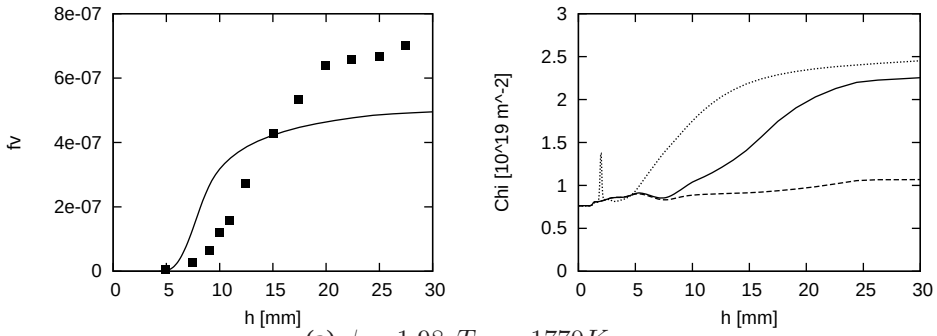

(a) $\phi = 1.98, T_{10} = 1770K$

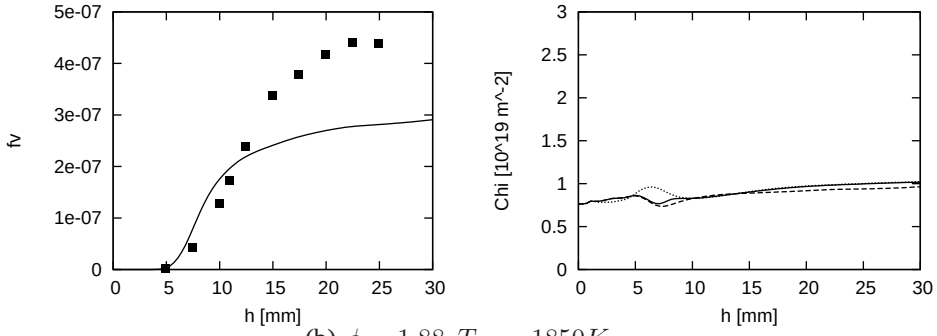

(b) $\phi = 1.88, T_{10} = 1850K$

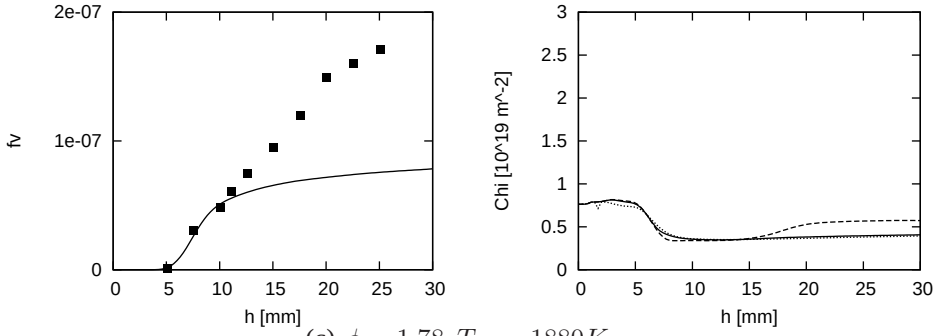

(c) $\phi = 1.78, T_{10} = 1880K$

Figure 6: Soot volume fractions (f_v) predicted with the current model and predicted density of active sites per unit soot surface (χ) (solid lines). Symbols are experiments [40]. For the actives, the dashed and dotted lines correspond to the contribution from the first and second delta functions, respectively.

hydrogenated sites (H), one can reconstruct the density of active sites as:

$$\chi = \frac{H}{S} \tag{38}$$

Together with the soot volume fraction, Fig. 6 also shows the density of active sites per unit soot surface area. It is observed that its mean value decreases with increasing temperature. It varies from below $\chi = 0.5 \times 10^{19} m^{-2}$ to around $\chi \approx 2.3 \times 10^{19} m^{-2}$. The contributions to the total active site density from the individual delta functions in the model, show that the surface reactivity is also a function of the particle size. For $\phi = 1.98$, the density of active sites is much larger for smaller particles corresponding to the first mode (first delta function) than for larger particles corresponding to the second mode (second delta function). However, for smaller equivalenece ratio flame the opposite is the case. This demonstrate the complex behaviour of this quantity, suggesting that a simple representation in terms of temperature and particle might not be possible.

4.3 Particle Diameter

Figure 7 compares the prediction of the diameter of the primary particles with the experimental values [40]. The particle diameters obtained from the current simulations are somewhat below the diameter measured from experiments. The first source of error certainly comes from the prediction of the soot volume fraction. For the three flames, the soot volume fraction was underestimated by up to a factor of two. This could directly translate into an increase of the diameter by a factor of $\sqrt[3]{2} \approx 1.3$, if we assume the number of primary particles to be correctly estimated. While this factor might explain most of the deviation between the computed and measured diameters, one has to question the validity of measuring the particle diameter from Transmission Electron Microscopy (TEM) pictures. The viscosity of soot particle is not well known and they exhibit characteristics of "liquidlike" materials [43]. As a consequence, after impacting the TEM grid, the soot aggregate might flatten and spread over a larger distance. Then, the measured diameter will be an upper limit of the true particle diameter. After taking those possible sources of error into account, the present model performs very well in predicting the primary particle diameters.

The three figures on the left of Fig. 7 also show the particle diameter of the two modes corresponding to the two delta functions used for the quadrature approximation. For most of the time, the first delta function remains located at a small diameter around $\mathrm{d_p} \approx 1\mathrm{nm}$ corresponding to the size of the first soot particles formed from collisions of two PAH species. The second mode reaches rapidly a steady state value between $10\mathrm{nm}$ and $20\mathrm{nm}$ depending on the flames. The mean diameter lies between the values for the two modes, but usually closer to the second mode. This comes from the fact that nucleation stops very rapidely in those flames. As a consequence, the magnitude of the first delta function tends to decrease and its weight is transferred to the second delta function.

Finally, Fig. 7 also shows the number of primary particles per aggregate (n_p). While there are no experimental values to compare with, one can estimate from the TEM pictures provided in Ref. [40] that this number lies somewhere between 10 to 100. In the current simulations, the number of primary particles per aggregate starts with one, since the first soot particles are assumed to be spherical. Later during the simulation, larger aggregates will form from the collision between smaller soot particles. Once again, the DQMOM allocates the first delta function to model the small particles ($n_p \approx 1$), while the second delta function is used for the large aggregates ($n_p \gg 1$).

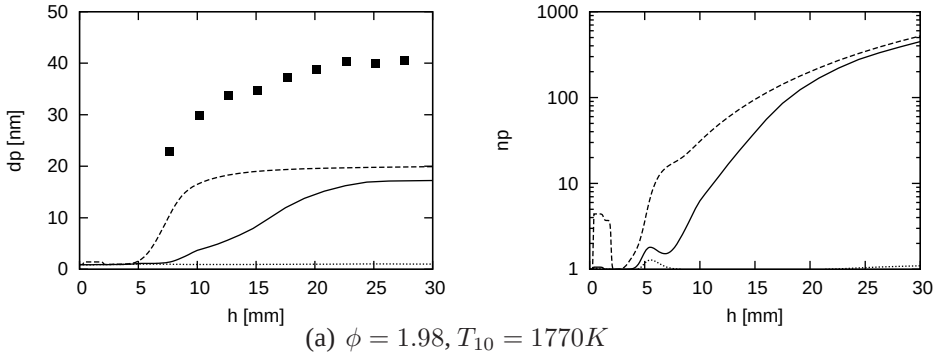

(a) $\phi = 1.98, T_{10} = 1770K$

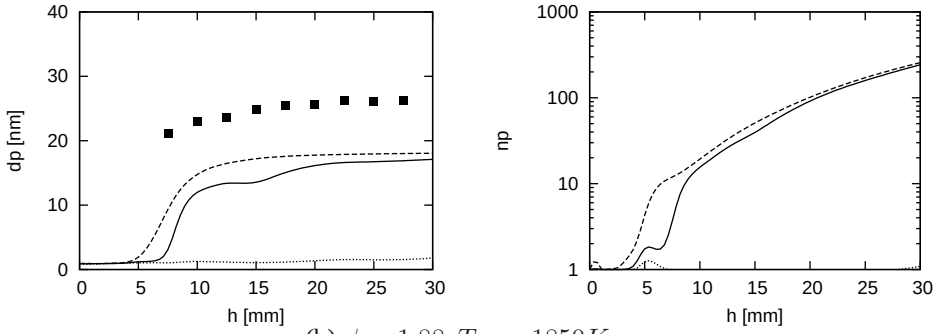

(b) $\phi = 1.88, T_{10} = 1850K$

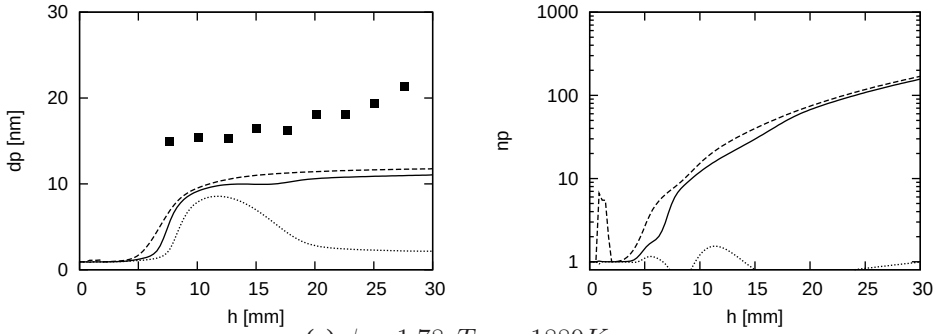

(c) $\phi = 1.78, T_{10} = 1880K$

Figure 7: Particle diameter (d_p) and number of primary particles per aggregate (n_p) predicted with the current model. Symbols are experiments [40].

5 Conclusion

In this work, a new parameter free aggregation model has been formulated. In this model, a soot particle is described as a fractal shaped aggregate composed of many spherical primary particles. The Direct Quadrature Method of Moments (DQMOM) is used to represent the number density function of soot particles. Three coordinates are used to characterize a soot aggregate: the total volume (V), the total surface area (S) and the total number of hydrogenated carbon sites on the soot surface (H). The VSH model is able to predict the soot volume fraction as well as the primary particle diameter for several flames with good accuracy. The reactivity of the surface, expressed by the density of active sites per unit soot surface, is shown to decrease when the temperature of the flame increases, thus giving a possible interpretation to the fall-off in soot yield at high temperature. Finally, the VSH model is able to provide an accurate prediction of the diameter of the primary particles without any adjustable parameters.

Acknowledgments

The authors gratefully acknowledge funding by the US Department of Energy within the ASC program.

References

[1] M. Schuetz, C. A.and Frenklach. *Proc. Comb. Inst.*, 29 (2002) 2307–2314.

[2] M Frenklach and H Wang. *Proc. Comb. Inst.*, 23 (1991) 1559–1566.

[3] U. O. Köylü, G. M. Faeth, T. L. Farias, and M. G. Carvalho. *Combust. Flame*, 100 (1995) 621–633.

[4] K. A. Jensen, J. M. Suo-Antilla, and L. G. Blevins. Characterization of soot properties in two-meter JP-8 pool fires. Technical Report SAND2005-0337, Sandia National Laboratories, 2005.

[5] P. Mitchell and M. Frenklach. *Proc. Comb. Inst.*, 27 (1998) 1507–1514.

[6] P. Mitchell and M. Frenklach. *Phys. Rev. E*, 67 (2003) –.

[7] P. Meakin. *J. Colloid Interface Sci.*, 96 (1983) 415–.

[8] M. Lattuada, H. Wu, and M. Morbidelli. *J. Colloid Interf. Sci.*, 268 (2003) 106–120.

[9] H.J. Schmid, S. Tejwani, C. Artelt, and W. Peukert. *J. Nanopart. Res.*, 6 (2004) 613–626.

[10] J Appel, H. Bockhorn, and M. Frenklach. *Comb. Flame.*, 121 (2000) 122–136.

[11] J. Singh, M. Blathasar, M. Kraft, and W. Wagner. *Proc. Comb. Inst.*, 30 (2005) 1457–1465.

[12] J. Singh, R. I. A. Patterson, M. Kraft, and H. Wang. *Combust. Flame*, 145 (2006) 117–127.

[13] B. Zhao, Z. Yang, M. V. Johnston, H Wang, A. S. Wexler, M. Balthasar, and M. Kraft. *Comb. Flame*, 133 (2003) 173–188.

[14] B. Zhao, Z. Yang, Z. Li, , M. V. Johnston, and H Wang. *Proc. Comb. Inst.*, 30 (2005) 1441–1448.

[15] D. L. Marchisio and R. O. Fox. *J. Aerosol Sci.*, 36 (2005) 43–73.

[16] G. P. Smith, D. M. Golden, F. Frenklach, N. W. Moriarty, B. Eiteneer, M. Goldenberg, C. T. Bowman, R. K. Hanson, S. Song, W. C. Jr. Gardiner, V. V. Lissianski, and Z. Qin. http://www.me.berkeley.edu/grimech/.

[17] B. Eiteneer and M. Frenklach. *Int. J. Chem. Kinet.*, 35 (2003) 391–414.

[18] B. Eiteneer and M. Frenklach. *Int. J. Chem. Kinet.*, 32 (2000) 589–614.

[19] H. Wang and M. Frenklach. *J. Phys. Chem.*, 97 (1993) 3867–3874.

[20] H. Wang and M. Frenklach. *J. Phys. Chem.*, 98 (1994) 11465–11489.

[21] H. Wang and M. Frenklach. *Comb. Flame*, 110 (1997) 173–221.

[22] G. Blanquart and H. Pitsch. *J. Phys. Chem. A*, (2007) (submitted).

[23] S. J. Harris and A. M. Weiner. *Combust. Sci. Technol.*, 31 (1983) 155–167.

[24] R.G. Gordon. *J. Math. Phys.*, 9 (1968) 655.

[25] A. Violi, A. F. Sarofim, and T. N. Truong. *Comb. Flame*, 126 (2001) 1506–1515.

[26] A. Violi, A. F. Sarofim, and T. N. Truong. *Comb. Sci. Tech.*, 174 (2002) 205–222.

[27] A. Violi. *Comb. Flame*, 139 (2004) 279–287.

[28] H Richter, O. A. Mazyar, R. Sumathi, W. H. Green, J. B. Howard, and J. W. Bozzelli. *J. Phys. Chem. A*, 105 (2001) 1561–1573.

[29] F. Goulay and S. R. Leone. *J. Phys. Chem. A*, 110 (2006) 1875–1880.

[30] A. Kazakov and M Frenklach. *Comb. Flame*, 114 (1998) 484–501.

[31] S. E. Pratsinis. *J. Colloid Interface Sci.*, 124 (1988) 416–428.

[32] F. E. Kruis, K. A. Kusters, S. E. Pratsinis, and B. Scarlett. *Aerosol Sci. Technol.*, 19 (1993) 514–526.

[33] A. M. Mebel, M. C. Lin, T. Yu, and K Morokuma. *J. Phys. Chem. A*, 101 (1997) 3189–3196.

[34] I. V. Tokmakov and M. C. Lin. *J. Phys. Chem. A*, 106 (2002) 11309–11326.

[35] J. A. Miller and S. J. Klippenstein. *J. Phys. Chem. A*, 107 (2003) 7783–7799.

[36] M. Frenklach, C. A. Schuetz, and J. Ping. *Proc. Combust. Inst.*, 30 (2005) 1389–1396.

[37] M. Frenklach. *Proc. Combust. Inst.*, 26 (1996) 2285–2293.

[38] J. Nagle and R. F. Strickland-Constable. In Pergamon, editor, *5th Carbon Conference*, Vol. 1, pages 154–164. Oxford, 1962.

[39] A. M. Nienow, J. T. Roberts, and M. R. Zachariah. *J. Phys. Chem. B*, 109 (2005) 5561–5568.

[40] F. Xu, P. B. Sunderland, and G. M. Faeth. *Combust. Flame*, 108 (1997) 471–493.

[41] H. Pitsch. FlameMaster, a C++ computer program for 0D combustion and 1D laminar flame calculations.

[42] H. Bohm, D. Hesse, H. Jander, B. Luers, J. Pietscher, H. GG. Wagner, and M. Weiss. *Proc. Comb. Inst.*, 22 (1988) 403–411.

[43] B. Oktem, M. P. Tolocka, B. Zao, H. Wang, and M. V. Johnston. *Comb. Flame.*, 142 (2005) 364–373.